

Stereospecific modulation of dimeric rhodopsin

Tamar Getter,^{*,†,1} Sahil Gulati,^{*,†,‡} Remy Zimmerman,^{*} Yuanyuan Chen,^{§,¶} Frans Vinberg,^{||} and Krzysztof Palczewski^{*,†,‡,2}

^{*}Department of Ophthalmology, Gavin Herbert Eye Institute and [†]Department of Physiology and Biophysics, University of California–Irvine, Irvine, California, USA; [‡]Department of Pharmacology, Case Western Reserve University, Cleveland, Ohio, USA; [§]Department of Ophthalmology, School of Medicine and [¶]McGowan Institute of Regenerative Medicine, University of Pittsburgh, Pittsburgh, Pennsylvania, USA; and ^{||}Department of Ophthalmology and Visual Sciences, University of Utah, Salt Lake City, Utah, USA

ABSTRACT: The classic concept that GPCRs function as monomers has been challenged by the emerging evidence of GPCR dimerization and oligomerization. Rhodopsin (Rh) is the only GPCR whose native oligomeric arrangement was revealed by atomic force microscopy demonstrating that Rh exists as a dimer. However, the role of Rh dimerization in retinal physiology is currently unknown. In this study, we identified econazole and sulconazole, two small molecules that disrupt Rh dimer contacts, by implementing a cell-based high-throughput screening assay. Racemic mixtures of identified lead compounds were separated and tested for their stereospecific binding to Rh using UV-visible spectroscopy and intrinsic fluorescence of tryptophan (Trp) 265 after illumination. By following the changes in UV-visible spectra and Trp265 fluorescence *in vitro*, we found that binding of *R*-econazole modulates the formation of Meta III and quenches the intrinsic fluorescence of Trp265. In addition, electrophysiological *ex vivo* recording revealed that *R*-econazole slows photoresponse kinetics, whereas *S*-econazole decreased the sensitivity of rods without effecting the kinetics. Thus, this study contributes new methodology to identify compounds that disrupt the dimerization of GPCRs in general and validates the first active compounds that disrupt the Rh dimer specifically.—Getter, T., Gulati, S., Zimmerman, R., Chen, Y., Vinberg, F., Palczewski, K. Stereospecific modulation of dimeric rhodopsin. *FASEB J.* 33, 000–000 (2019). www.fasebj.org

KEY WORDS: GPCR dimerization · high-throughput screening · G-protein-coupled receptors · chromophore · isomerization

GPCRs are the largest family of membrane proteins involved in signal transduction pathways influencing physiologic and pathophysiological processes (1–4). GPCRs are heptahelical receptors with an extracellular N terminus, an intracellular C terminus, and 7 lipophilic

transmembrane (TM) regions linked by extracellular and intracellular loops. The rhodopsin (Rh)-like GPCRs are one of the most important drug targets (5) characterized by a large variety of ligands by which they can transduce extracellular signals (6–8). Rh is a light-sensitive GPCR that is composed of a covalently bound 11-*cis*-retinal chromophore. Upon absorption of a photon, 11-*cis*-retinal isomerization initiates a series of conformational changes that lead to the formation of Rh photointermediates (9–11). The metarhodopsin (Meta) II state (λ_{\max} : 380 nm) is an active Rh intermediate that binds and activates the heterotrimeric G-protein transducin (G_t) (12). The Meta II state exists in equilibrium with its inactive precursor, Meta I (λ_{\max} : 480 nm). Under physiologic conditions, Meta II is formed within milliseconds and on the time scale of min then decays by hydrolysis of the retinal Schiff base into opsin and free all-*trans*-retinal. Thermal isomerization of the Schiff base from *anti* to *syn* results in Meta III (λ_{\max} : 465 nm) that is photoconvertible to Meta II (13–15).

The precise organization of GPCRs is crucial for proper extracellular signal transduction and function (16, 17). The first structural evidence supporting Rh dimerization was provided by atomic force microscopy studies, where Rh was the only GPCR whose native oligomeric arrangement was revealed (18–21). This powerful imaging technique

ABBREVIATIONS: β 2AR, β -2 adrenergic receptor; β -gal, β -galactosidase; BRET, bioluminescence resonance energy transfer; CHAPS, 3-[(3-cholamidopropyl) dimethylammonio]-1-propanesulfonate; CNBr, cyanogen bromide; DDM, *n*-dodecyl β -D-maltoside; EA, enzyme acceptor; ERG, electroretinogram; FBS, fetal bovine serum; G_t , G-protein transducin; GTP γ S, guanosine 5'-O-[γ -thio]triphosphate; HEK293, human embryonic kidney 293 cells; HEPES, 4-(2-hydroxyethyl)-1-piperazineethanesulfonic acid; HTS, high-throughput screening; LMNG, lauryl maltose-neopentyl glycol; MES, 2-(*N*-morpholino)ethanesulfonic acid; Meta, metarhodopsin; PK, ProLink peptide donor; QC, quality control; Rh, rhodopsin; r_{\max} , maximal response amplitude; ROS, rod outer segment; S/B, signal-to-background; SAR, structure-activity relationship; TM, transmembrane; Trp, tryptophan; U2OS, human osteosarcoma (U2OS)

¹ Correspondence: Department of Ophthalmology, Gavin Herbert Eye Institute, University of California–Irvine, 850 Health Sciences Rd., Irvine, CA 92697, USA. E-mail: tgetter@uci.edu

² Correspondence: Department of Ophthalmology, Gavin Herbert Eye Institute, University of California–Irvine, 850 Health Sciences Rd., Irvine, CA 92657, USA. E-mail: kpalczew@uci.edu

doi: 10.1096/fj.201900443RR

This article includes supplemental data. Please visit <http://www.fasebj.org> to obtain this information.

demonstrated that Rh assembles in rows of dimers and was confirmed by cryo-electron tomography of rod outer segments (ROS) in almost native state conditions (22). However, the functional role of Rh dimerization remains an open question because, in biochemical assays, monomeric and dimeric Rh structures are fully capable of signal transduction (23). As a result, Rh dimerization has attracted major interest to scientists in vision research and in the field of GPCRs.

Dimerization deficiency does not result in the complete loss of Rh functionality; rather, it might be important for ROS disc formation, G-protein activation, or Rh deactivation *in vivo*. The inability to generate appropriate high-order Rh structures in disc membranes could possibly affect the stability of ROS. Various approaches have been used to better understand the functional significance of Rh dimerization, including 1) *in silico* studies to predict residues involved in dimer formation (24, 25), 2) *in vitro* studies using synthetic peptides derived from Rh TM domains to disrupt Rh dimerization (26), 3) biochemical or structural approaches (27–29), and 4) *in vivo* studies targeting the Rh dimer interface (30, 31).

Small molecules disrupting the formation of Rh dimers can serve as useful tools to understand the physiologic role of Rh dimerization. In this study, we developed a robust cell-based high-throughput screening (HTS) assay using luminescence as the detection method. This highly sensitive assay employs the β -galactosidase (β -gal) complementary effect of two separated subunits each of which is fused to opsin apoprotein. A complementary cell-based bioluminescence resonance energy transfer (BRET) assay was used in combination with UV-visible assays to validate hit compounds identified from HTS. This HTS methodology could be adapted to other GPCR systems and we expect that the strategy developed for our investigation will have applications for the study of other GPCRs or membrane receptors to allow for a better understanding of their specific dimerization mechanisms.

MATERIALS AND METHODS

Chemicals

The Gal-Screen β -gal reporter gene assay system for mammalian cells was purchased from Thermo Fisher Scientific (Waltham, MA, USA). The Spectrum Collection containing 2400 pharmacologically active compounds was purchased from MicroSource Delivery Systems (Gaylordsville, CT, USA). 9-*cis*-Retinal, dinitrophenol, aurin, phenazopyridine, sulfanitran, nitroprusside, levosimendan, acriflavine, ecanazole, sulconazole, 4-methylumbelliferyl- β -D-galactopyranoside, *n*-dodecyl β -D-maltoside (DDM), 3-[3-(cholamidopropyl) dimethylammonio]-1-propane-sulfonate (CHAPS), lauryl maltose-neopentyl glycol (LMNG), hydroxylamine, guanosine 5'-O-[γ -thio]triphosphate (GTP γ S), carbinoxamine [structure-activity relationship (SAR) 8], 6-(4-chlorophenyl)-3-morpholinone (SAR-12), 1-(4-chlorobenzyl)-1H-imidazole (SAR-1), 4-chlorobenzyl 2-(1H-imidazol-1-yl)-1-phenylethyl ether (SAR-21), 1-dimethylamino-2-chlorobenzoate hydrochloride (SAR-16), 2-(4-chlorophenyl)morpholine (SAR-10), 1-(2,4-dichlorobenzyl)-1H-imidazole (SAR-7), 1-(2,4-dichlorophenyl)-2-imidazol-1-yl-ethanol (SAR-9), 2-[(3,4-dichlorobenzyl) sulfanyl]-1-methyl-1H-imidazole (SAR-15), and imazalil (SAR-11) were obtained from MilliporeSigma (Burlington, MA,

USA). Isoconazole (SAR-6), LYN-1604 (SAR-17), fenticonazole (SAR-3), SKF-96365 (SAR-13), itraconazole metabolite (SAR-18), itraconazole (SAR-19), terconazole (SAR-20), sertaconazole (SAR-4), miconazole (SAR-5), tioconazole (SAR-14), and ketoconazole (SAR-2) were purchased from Abovchem (San Diego, CA, USA). BRET assay substrate pivaloyloxymethyl acetoxycocelenterazine h was obtained from Dalton Research Molecules (Toronto, ON, Canada). Rh-derived TM5 peptide (SKSKSKNESFVIYMFVVHFIPLIVIFFSYGQLVFW-NH₂) was custom synthesized by EZBiolab (Carmel, IN, USA).

Generation of stable U2OS opsin–enzyme acceptor and donor expressing cell lines

Constructs of PathHunter Rh–enzyme acceptor (EA) and Rh-ProLink peptide donor (PK) adherent retroviruses were generated by DiscoverX (Fremont, CA, USA) for the ligand-induced β -gal complementary opsin dimerization assay. Human osteosarcoma (U2OS) cells were plated 1 d prior to retroviral transfection. Cells were detached from the tissue culture flask with 0.25% trypsin (Thermo Fisher Scientific) and resuspended in DMEM, a high glucose medium containing 10% fetal bovine serum (FBS) and 1% penicillin-streptomycin 10,000 U/ml (Thermo Fisher Scientific). Cells were then counted with a hemocytometer (Thermo Fisher Scientific) and diluted to about 5×10^4 cells/ml. The cell diluent was dispensed into a 6-well cell culture plate at 2 ml/well and incubated overnight at 37°C in 5% CO₂. The following day, 0.5 ml cell culture medium was removed and 0.5 ml opsin-EA 16K26BG retroviruses (DiscoverX) were added, followed by a 48-h incubation period at 37°C in 5% CO₂. Transduced cells were transferred to a 48-well cell culture dish containing 400 μ l/well of 5×10^4 cells/ml medium. For positive selection of opsin-EA-expressing cells, 300 μ g/ml hygromycin B (DiscoverX) was used and incubated for 10 d under selection at 37°C in 5% CO₂.

Expression of the opsin-EA fusion was confirmed by immunoblotting with the mouse monoclonal B630 anti-Rh antibody (molecular mass of opsin-EA, 150 kDa) and by immunostaining with the B630 anti-Rh antibody, PathHunter anti-EA antibody (DiscoverX), and the Cy3 conjugated goat anti-mouse IgG. Fluorescence microscopy using an Operetta high-content imaging system (PerkinElmer, Waltham, MA, USA) was used. A stable U2OS cell line expressing opsin-EA was used for opsin-PK fusion to generate U2OS opsin-EA and opsin-PK expressing cell lines. U2OS opsin-EA cells were plated into a 6-well cell culture plate and incubated overnight at 37°C in 5% CO₂. Cells were then infected with opsin-PK 16K12BG retroviruses (DiscoverX) and incubated for 48 h at 37°C in 5% CO₂. Transfected cells were transferred to a 48-well plate and treated with 500 μ g/ml neomycin (DiscoverX) for positive selection of the opsin-PK fusion protein in U2OS opsin-EA cells. Expression of both opsin-EA and opsin-PK fusion proteins was confirmed by immunoblotting with the mouse monoclonal B630 anti-Rh antibody (molecular mass of opsin-PK, 41 kDa, opsin-EA/PK, 191 kDa) and immunostaining with PathHunter anti-PK/PL antibody (DiscoverX) as well as by subsequently performing a functional response study.

Immunoblotting

U2OS opsin-EA and opsin-PK stable cells were collected, pelleted at 1000 *g*, and washed twice with 1.05 mM KH₂PO₄, 155.1 mM NaCl, and 2.96 mM Na₂HPO₄·7H₂O, pH 7.4 (PBS). Cell pellets were resuspended in 30 μ l PBS supplemented with 0.5 μ l benzozonase (MilliporeSigma) for 5 min, followed by sonication at room temperature in a water bath for 5 min. This solution was then centrifuged at 16,000 *g* for 15 min at 4°C. Total protein from

cell lysates (30 μg) was separated by SDS-PAGE followed by transfer onto a PVDF membrane. The PVDF membrane, after blocking with 5% unsaturated milk, was incubated with mouse monoclonal B630 anti-Rh monoclonal antibody (stock solution of 2 mg/ml) at a dilution of 1:1000. Immunoblots were developed with a Novex BCIP/NBT Detection Kit (Thermo Fisher Scientific).

Immunostaining

U2OS opsin-EA and opsin-PK stable cells were adjusted to 1×10^5 cells/ml and dispensed into a 384-well black clear bottom plate (PerkinElmer) at 40 μl /well and cultured overnight at 37°C, 5% CO₂. As a reference, U2OS and U2OS opsin-EA expressing cells were used. Cells were washed once with PBS and then fixed with 4% paraformaldehyde (MilliporeSigma) for 15 min at 20°C followed by 3 washes with PBS and incubation with PBST (0.3% Tween 20) containing 5% goat serum for 20 min at 20°C. Cells were subsequently incubated with 20 μl of B630 antibody at 2.1 $\mu\text{g}/\text{ml}$ (1:2000 of stock solution ~ 16 mg/ml) in PBST overnight at 20°C, or PathHunter anti-PK at 2.1 $\mu\text{g}/\text{ml}$ (1:50 of stock solution ~ 16 mg/ml) or PathHunter anti-EA at 2.1 $\mu\text{g}/\text{ml}$ (1:2500 of stock solution ~ 16 mg/ml) (DiscoverX). The following day, the cells were washed with PBS and incubated with 1:500 diluted Cy3 conjugated goat anti-mouse IgG (stock solution of 1.5 $\mu\text{g}/\text{ml}$) in PBST for 40–60 min at 20°C. After cells were washed 3 times with PBST, 40 μl /well of 10 μM DAPI solution in PBS (Thermo Fisher Scientific) was added to the 384-well plate. Images were taken with an Operetta high-content imaging system along with an analysis implemented by Harmony high-content imaging and analysis software (PerkinElmer).

β -Gal HTS fragment complementation assay

On d 1, cultured U2OS opsin-EA and opsin-PK cells were detached with 0.25% trypsin (Thermo Fisher Scientific) and resuspended in DMEM, a high glucose medium containing 10% FBS and 1% penicillin-streptomycin 10,000 U/ml followed by a dilution to 2×10^5 cells/ml in culture medium. The cell diluent of 20 μl /well was dispensed into a white ViewPlate-384 with an optically clear bottom, tissue culture treated, sterile plates (PerkinElmer) using the EL406 plate dispenser (BioTek Instruments, Winooski, VT, USA). Columns 3–24 were used for seeding U2OS opsin-EA and opsin-PK expressing cells. In column 1–2, U2OS cells and U2OS opsin-EA expressing cells were dispensed in a similar manner serving as controls. The plates were cultured overnight at 37°C in 5% CO₂. On d 2, under a dim red light, cells were treated with 5 μl /well of 9-*cis*-retinal (MilliporeSigma) solution to achieve a 7.5 μM final concentration with the EL406 plate dispenser. Plates were covered with aluminum foil and cultured overnight at 37°C in 5% CO₂. On d 3, cells were treated with the pharmacologically active library of 2400 compounds (MicroSource) using a Janus automated workstation (PerkinElmer). Each well was treated with 144 nl of 10 mM compound stock library to achieve a final concentration of 57.6 μM . Columns 1–2 and 23–24 were used as controls (no compound treated wells), followed by incubation overnight in the dark at 37°C and 5% CO₂. On d 4, cells were treated with Galacton-Star chemiluminescent substrate (Thermo Fisher Scientific) and the reaction buffer was prepared per Gal-Screen System instructions. The prepared substrate was dispensed into the 384-well plates at 23 μl /well with the EL406 plate dispenser, and only columns 1–23 were treated, whereas column 24 was used as a nonsubstrate control. The plates were covered with foil and incubated at 20°C for 2 h, followed by luminescence reading with

the EnSpire multimode plate reader (PerkinElmer). All hit compounds were retested in triplicate ranging from 320 μM to 2.4 nM concentrations (32). The quality control (QC) parameters, the signal-to-background (S/B) ratio and Z' values were calculated as $S/\text{Bratio} = \text{mean}_{100\% \text{ control}} / \text{mean}_{0\% \text{ control}}$ and $Z' = 1 - 3 \times (\text{SD}_{0\% \text{ control}} + \text{SD}_{100\% \text{ control}}) / |\text{mean}_{100\% \text{ control}} - \text{mean}_{0\% \text{ control}}|$ (33). Here, the 100% control consisted of opsin-EA expressing cells, and the 0% control had opsin-EA/PK expressing cells. The QC parameters demonstrated an S/B ratio $>168 \pm 22$ and $Z' >0.58 \pm 0.15$.

Venus and *Renilla* luciferase BRET assay

Stable expressing human embryonic kidney 293 cells opsin-Rluc and opsin-Venus cell lines were generated as previously described by Jastrzebska *et al.* (26) by sequential incorporation of the opsin-Rluc pCDNA3.1Zeo and opsin-Venus pCDNA3.1Zeo vectors. HEK-293 (opsin-Rluc and opsin-Venus) stable cells were used for secondary opsin dimerization assay confirmation. On d 1, cultured cells were detached from 150 mm tissue culture plates by 0.05% trypsin (Thermo Fisher Scientific) and resuspended in culture medium. The suspended cells were diluted to 2×10^5 cells/ml containing DMEM, a high glucose medium with 10% FBS and 1% penicillin-streptomycin 10,000 U/ml, and 20 μl /well of cell diluent was dispensed into a white optically clear bottom ViewPlate-384 with an EL406 plate dispenser. Cells were cultured overnight at 37°C in 5% CO₂. On d 2, under a dim red light, cells were treated with 9-*cis*-retinal as described in the β -gal fragment complementation assay. On d 3, cells were treated with DMSO or 1 μM TM5 peptide (SKSKSKNESFVYMFVVH-FIIPLVIVFFSYGQLVFW-NH₂; EZBiolab) dissolved in 0.2 mM DDM serving as controls along with hit compounds ranging from 320 μM to 2.4 nM concentrations using a Janus automated workstation. On d 4, the culture medium was aspirated and replaced with 80 μl /well of PBS with the EL406 plate dispenser. Pivaloyloxymethyl acetoxycoumarin (Dalton Research) was diluted in PBS to 600 μM concentration, and 10 μl /well were dispensed into a 384-well plate followed by incubation at 20°C for 40 min (34). Dual luminescence readings at 480 and 530 nm were performed using a SpectraMax L plate reader with the BRET1 filter set (Molecular Devices, Sunnyvale, CA, USA).

β -Gal activation assay

β -gal (MilliporeSigma) was dissolved in 5 mM sodium phosphate buffer, pH 7.4 and dispensed into a black ViewPlate-384, with an optically clear bottom at 20 μl /well to achieve the final concentration of 60 μM . In the activity assay, β -gal solution was incubated with various concentrations of the hit compounds (ranging from 320 μM to 2.4 nM) in triplicate for 2.5 h on ice. The fluorogenic substrate (35), 4-methylumbelliferyl- β -D-galactopyranoside (MilliporeSigma) was added at 20 μl /well to achieve the final concentration of 1 mM. As a control experiment, the enzymatic activity of β -gal also was monitored with 0.01% DMSO treatment. The samples were then incubated for 2 h on ice, and the enzymatic activity was monitored at 455 nm with an EnSpire multimode plate reader (PerkinElmer).

Cell viability assay

On d 1, a cultured U2OS opsin-EA and opsin-PK cell line was detached from the tissue culture flask with 0.25% trypsin (Thermo Fisher Scientific) and resuspended in culture medium followed by dilution to 2.6×10^4 cells/ml. The cell diluent was dispensed into a white ViewPlate-384 at 20 μl /well with column 1 containing only medium to serve as a control.

This assay is based on the lack of ATP production resulting in cell death. On d 2 and 3, cells were treated with 9-*cis*-retinal and hit compounds ranging from 20 to 0.1 μM in triplicate. On d 4, ATP levels were measured by incubation with 25 μl /well of CellTiter-Glo reagent (Promega, Madison, WI, USA). Treated cells were incubated at 20°C for 1 h and luminescence was recorded with a SpectraMax L plate reader (Molecular Devices).

Rh purification

Bovine ROS were isolated and prepared as previously described in Papermaster (36). ROS washed with isotonic and hypotonic buffers were used for Rh purification (in the dark under a dim red light with >670 nm observance) as previously described (37–39). Briefly, for Rh extractions, native Rh membranes were solubilized with a zinc/alkyl-glucoside and centrifuged at 100,000 *g* for 40 min. Supernatants were loaded on a 1D4-coupled cyanogen bromide (CNBr)-activated Sepharose 4B column and washed with buffer containing 10 mM 2-(*N*-morpholino)ethanesulfonic acid (MES), pH 6.4, 100 mM NaCl, and 0.02% DDM. Finally, purified Rh was eluted with 0.5 mg/ml of TETSQVAP peptide recognizing the C-terminal sequence of Rh (38).

Chromatographic condition

The racemic mixtures of ecanazole and sulconazole (MilliporeSigma) were separated by an Agilent 1100 HPLC system (Agilent Technologies, Santa Clara, CA, USA) at a flow rate of 1 ml/min. Separation was achieved with a cellulose tris 3,5-dimethylphenylcarbamate Chiralcar column (Chiral Technologies, West Chester, PA, USA). The mobile phase used in this study was hexane-2 propanol-diethylamin (485:14:1 v/v/v) and the detection was carried out at 280 nm. (Retention times: *R*-econazole 40 min and *S*-econazole 48 min/*R*-sulconazole 100 min and *S*-sulconazole 140 min). Enantiomer characterization was determined as previously described in Aboul-Enein and Ali (40).

Spectroscopy

Rh solubilized at 0.68 mg/ml in 20 mM bis-tris propane, pH 6.9, 100 mM NaCl, 1 mM DDM buffer was incubated (final Rh concentration was 1.36 μM) with 50 μM of *R*-econazole, *S*-econazole, *R*-sulconazole, or *S*-sulconazole for 10 min at 20°C and centrifuged at 1000 *g* for 5 min. Absorption spectra of Rh with and without the compounds were then measured with a Cary 50 UV-visible spectrophotometer (Varian Medical Systems, Palo Alto, CA, USA). Photobleaching was carried out with a 150-W fiber light delivered through a 480–520 nm band pass filter (Chroma Technology, Bellows Falls, VT, USA) for 10–40 s. For detergent screening, Rh was solubilized in different detergents: LMNG, DDM, and CHAPS at 1 mM concentration for 10 min at 20°C. Photobleaching experiments of Rh in 20 mM bis-tris propane, pH 6.9, 100 mM NaCl, 1 mM DDM/LMNG/CHAPS buffers were performed as described in this section.

Hydroxylamine reactivity

Hydroxylamine reactivity of the dark and light states of Rh treated with *R*-econazole was measured as described above for the photobleaching experiments. The formation of all-*trans*-retinal (λ_{max} : 360 nm) was carried out with 5 mM NH_2OH treated Rh and Rh *R*-econazole incubated for 10 min at 20°C and centrifuged at 1000 *g* for 5 min (41).

Meta II decay assay

Rh treated with *R*-econazole and *S*-econazole was analyzed with a L55 luminescence spectrophotometer (PerkinElmer) operating at excitation and emission wavelengths of 300 and 335 nm, respectively. Solubilized Rh at 1.36 μM was incubated with 50 μM of *R*-econazole or *S*-econazole for 10 min at 20°C and centrifuged at 1000 *g* for 5 min. Samples were bleached for 10 s with a fiber light delivered through a 480–520 nm long-pass wavelength filter (Chroma Technology) before the fluorescence measurements were acquired over 3000 s.

Purification of G_t

Heterotrimeric G_t was prepared as previously described in Gulati *et al.* (42). Briefly, bovine ROS were suspended in isotonic buffer containing 20 mM 4-(2-hydroxyethyl)-1-piperazineethanesulfonic acid (HEPES), pH 7.5, 100 mM NaCl, 1 mM DTT, and 5 mM MgCl_2 and centrifuged at 31,000 *g* for 25 min at 4°C. The pellet was homogenized in a hypotonic buffer containing 5 mM HEPES, pH 7.5, 1 mM EDTA and 1 mM DTT and centrifuged at 40,000 *g* for 30 min at 4°C multiple times. The clear supernatant was dialyzed with a buffer containing 10 mM HEPES, pH 7.5, 2 mM MgCl_2 , and 1 mM DTT for 3 h at 4°C. The purification of heterotrimeric G_t was performed with a C10/10 column (GE Healthcare, Waukesha, WI, USA) and the eluate containing heterotrimeric G_t was concentrated and loaded onto a Superdex 200 10/300 GL column (GE Healthcare). A concentrated fraction of heterotrimeric G_t containing about 2 mg/ml was used for further analyses.

G_t activation assay

The intrinsic fluorescence increase was measured with a L55 luminescence spectrophotometer (PerkinElmer) at excitation and emission wavelengths of 300 and 335 nm, respectively. Rh at 50 nM concentration was preincubated with 0.2 μM of *R*-econazole or *S*-econazole for 10 min at 20°C. This was followed by the addition of 500 nM G_t and 300 μM $\text{GTP}\gamma\text{S}$ (MilliporeSigma) and incubation for 3 min at 20°C. The $\text{GTP}\gamma\text{S}$ -induced complex dissociation was measured by photobleaching the samples for 10 s with a fiber light delivered through a 480–520 nm long-pass wavelength filter (Chroma Technology) followed by the fluorescence measurements. Initial G_t activation rates were monitored for the first 100 s (38, 43, 44).

Ex vivo electroretinography

Photoreceptor responses to light were measured using an *ex vivo* electroretinography method as previously described in Vinberg *et al.* (45). Briefly, wild-type mice (C57Bl/6J, 2–3 mo.) were dark-adapted overnight and euthanized by CO_2 asphyxiation and cervical dislocation just before eye enucleation and dissection of the retinas. Isolated retinas with no retinal pigment epithelium were mounted on a custom-built specimen holder (46) where they were superfused at 1 ml/min with Ames' medium (MilliporeSigma) at 36°C. Ames' was supplemented with 40 μM DL-AP4 (Tocris Bioscience, Bristol, United Kingdom) and 100 μM BaCl_2 to isolate the photoreceptor component of the electroretinogram (ERG) signal. Electrical responses were elicited by calibrated (photodiode FDS1000; Thorlabs, Newton, NJ, USA) 1 ms flashes of green (530 nm) light ranging from 100 to 4000 photons μm^{-2} . Because retinas were dark-adapted and flash intensities were low, these responses originate almost exclusively from rod activity in the rod-dominant mouse retina. To determine the effects of econazole and its enantiomers on rod

photoreceptor function, we either added 500 μM econazole, *R*-econazole, or *S*-econazole in perfusion medium or incubated retinas for 5–6 h in Ames' containing 500 μM econazole, *R*-econazole, or *S*-econazole before electroretinography experiments. We used 1000X (500 mM) stock solutions of econazole, *R*-econazole, or *S*-econazole in DMSO to prepare all Ames' buffers that contained different enantiomers of econazole. Control solutions were always supplemented with 0.1% DMSO. Maximal response amplitudes (r_{max}) were measured at the plateau after the initial peak present in responses to the brightest flash of light. Light sensitivities of rods exposed to econazole, *R*-econazole, *S*-econazole, or control solutions were compared by measuring the peak amplitude of responses to the dimmest flash divided by r_{max} .

Statistical analyses

All experiments were performed in triplicate. Data were presented as means \pm SD, and statistical analyses were performed using a Student's *t* test. Values of $P \leq 0.05$ were considered statistically significant.

RESULTS

Identifying disrupters of Rh dimerization *in vitro*

To understand the physiologic importance of Rh self-association, an HTS cell-based assay was used to screen compounds for their ability to disrupt Rh dimerization. A U2OS stable cell line was generated expressing both opsin fused with the EA subunit of β -gal and opsin fused with the small peptide PK fragment enzyme donor complementary subunit of β -gal (32, 47, 48). Cells expressing both opsin-fused proteins were regenerated with 9-*cis*-retinal to form fully functional Rh. Rh dimerization then brings both fragments of β -gal into proximity to reconstitute the active enzyme capable of hydrolyzing substrate and generating a chemiluminescent signal (Fig. 1A). Expression of opsin-EA and opsin-PK fusion proteins was detected by immunoblotting and immunostaining confirming that the expressed opsins were localized to the plasma membrane (Fig. 1B). A total of 2400 compounds, including 1600 US Food and Drug Administration–approved drugs and 800 natural substances and pharmacologically active compounds were screened initially at a concentration of 57.6 μM . A Z' factor of 0.58 ± 0.15 and an S/B ratio of 168 ± 22 were used as thresholds for identifying hit compounds (33). The Z' factor reflects the quality of the HTS, whereby a score higher than 0.5 indicates a highly reliable and robust HTS assay. U2OS cells transfected with both opsin-EA and opsin-PK were used as a positive control representing the dimer formation (0% control), and an opsin-EA-only expressing cell line was used as a negative control representing the complete disruption of dimer (100% control) (Fig. 1C). The activity scores were calculated according to the equation $(\text{RLU}_{\text{compound}} - \text{RLU}_{\text{positive control}}) / (\text{RLU}_{\text{negative control}} - \text{RLU}_{\text{positive control}}) \times 100$ (where RLU is relative luminescence units). A total of 25 hits were identified with absolute cutline scores of $>50\%$ dimer disruption (Fig. 1D). All hits were then subjected to dose response assays in which 9 of the initial 25 hits showed

a dose-dependent activity with half maximal effective concentrations (EC_{50}) ranging from 2 to 25 μM (Supplemental Fig. S1).

To identify false-positives, a second assay was developed measuring the BRET effect between Rluc and Venus each fused to opsin (Fig. 2A). HEK293 cells expressing opsin-Rluc and opsin-Venus fusion proteins were regenerated with 9-*cis*-retinal and treated with 1 μM Rh-derived TM5 peptide (26, 49) solubilized in 0.2 mM DDM acting as a control (Fig. 2B). Due to the instability of the Rluc substrate Coelenterazine h, a derivative was used that provides a long-lasting light signal (34, 50). The commercial derivative is a protected form of Coelenterazine h that has esters added at the site of substrate oxidation. Once inside the cell, the protective groups are cleaved by intracellular esterases, generating the active Coelenterazine h, which then reacts with Rluc to produce light (Supplemental Fig. S2) (51). Of the 9 compounds identified in the first assay, 5 demonstrated a dose-dependent effect toward reducing the BRET signal in the second assay (Fig. 2C).

As a further control, a β -gal activity assay was used to counter screen and rule out false-positives affecting the activity of β -gal (34, 52). β -gal activity was then compared in the presence of 2 hit compounds, econazole and sulconazole, at various concentrations. No effect on the β -gal activity was observed, thus confirming that the activity observed earlier was not due to β -gal inhibition (Supplemental Fig. S3). Also, to eliminate the possibility that the decrease in the luminescence signal was not the result of compound cytotoxicity, hit compounds econazole and sulconazole were tested using the CellTiter-Glo luminescent cell viability assay. The results demonstrated that compounds econazole and sulconazole had no effect on cell viability (Supplemental Fig. S4) (53). The hit compounds, econazole and sulconazole, which share structures differentiated by only 1 atom (an oxygen substitution to sulfur) displayed similar EC_{50} values ranging from 13 to 24 μM in both β -gal and BRET assays, respectively.

SAR studies

SAR studies of the chemical scaffold were conducted using hit compounds econazole and sulconazole. Compound sulconazole is the sulfur analog of an ether functional group present in compound econazole. We screened the commercially available derivatives of hit compounds featuring a phenyl ring, linked by an ethane chain to the nitrogen of theazole ring. Of the 21 screened compounds, 6 derivatives interfered with Rh dimerization in a dose-dependent manner in both β -gal and BRET assays (Supplemental Figs. S5 and S6). SAR analysis suggested that the imidazole ring shared by all derivatives is essential for their activity. The derivatives lacking this feature, including SAR-8, SAR-10, SAR-11, SAR-12, SAR-15, SAR-16, SAR-17, SAR-18, SAR-19, and SAR-20 were incapable of disrupting Rh dimerization *in vitro* (Fig. 3). Addition of an orthochlorine in the phenyl ring (SAR-7) or a free hydroxyl

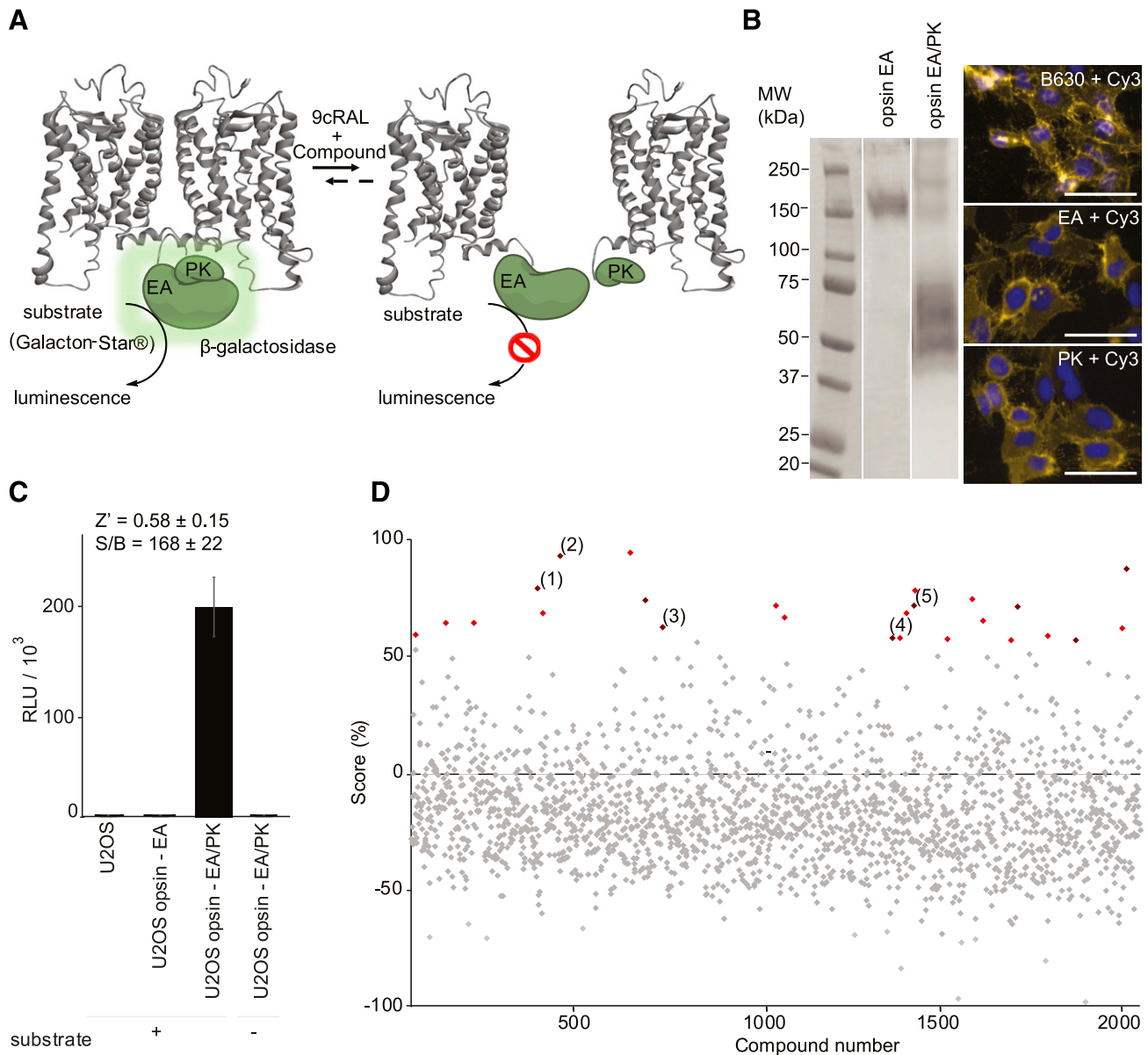


Figure 1. Rh dimerization disruption β -gal HTS. **A)** Illustration of the β -gal fragment complementary assay applied in HTS format. Expressed opsin-EA and opsin-PK proteins containing the large and small subunit of β -gal (EA and PK, green) were fused on the C-terminal of opsin (gray cartoon). Cells expressing opsin fusion proteins were regenerated by 9-*cis*-retinal before treatment with the screened compounds. Only when β -gal reconstitution is disrupted due to opsin separation is the activity quantified by its luminescence signal decrease. **B)** Immunoblot (left panel) of U2OS stable cells expressing the opsin-EA fusion protein (left lane) and the opsin-EA and PK fusion proteins (right lane). Scale bars, 20 μ m. Both were incubated with the B630 anti-Rh antibody that recognizes the N terminus of Rh. Immunostaining (right panel) of U2OS opsin-EA and PK stable cells treated with primary B630, EA, and PK antibodies and Cy3 secondary antibody. Yellow, opsin-EA/PK; blue, nuclease DAPI. **C)** The β -gal complementary activity in U2OS, U2OS opsin-EA, and U2OS opsin-EA/PK cells treated with and without Galacton-Star substrate. Values and error bars are means \pm sd from 16 biologic repeats. The HTS QC parameters S/B ratio and Z' (inset). **D)** Activity score plot of 2400 screened compounds in which 25 hits with Rh dimerization disruption effect were obtained (activity score \geq 50%, red). Activity scores were normalized by the luminescence measured by opsin-EA expressing cells and opsin-EA/PK expressing cells as 0 and 100% controls, respectively.

at the chiral carbon (SAR-9) drastically reduced the activity of SAR-1. However, the *para* positioned chloro group on the phenyl ring is essential for Rh dimerization disruption when comparing the activities of SAR-21, SAR-13, SAR-1, econazole, and sulconazole. Neither of the 1,2,4-triazole group derivatives (SAR-18, SAR-19, and SAR-20) or 2-chlorothiophene substitutes (SAR-14) showed any effect on Rh dimerization disruption. Finally, the comparison of

the imidazole-based hits revealed that the presence of the 1-(4-chlorophenethyl)-1H-imidazole scaffold was essential for Rh dimer disruption. Of all compounds tested, SAR-2 demonstrated the most promising β -gal and BRET effects with EC_{50} values of 3.62 and 4.48 μ M, respectively. Overall, these results suggested that a combination of 1-(4-chlorophenethyl)-1H-imidazole and a dioxolane scaffold is essential for the disruption of the Rh dimer.

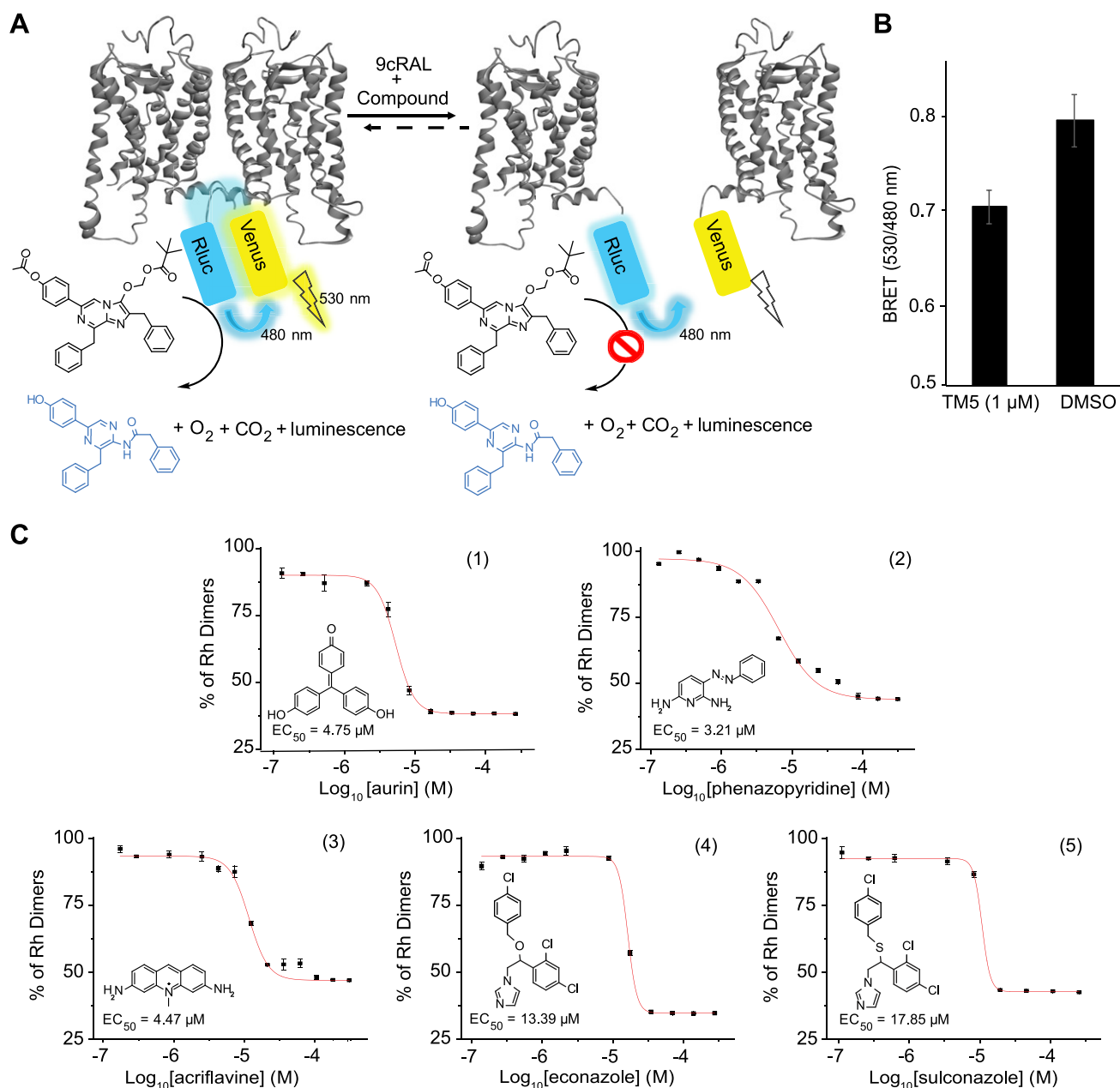


Figure 2. Complementary Rh dimerization BRET assay effects of identified hit compounds. *A*) Diagram of the opsin-Rluc (gray and blue) and opsin-Venus (gray and yellow) energy transfer reaction after addition of 9-*cis*-retinal, luciferase substrate (pivaloyloxymethyl acetoxycocenterazine h), and hit compound treatments. Disruption of Rh dimerization results in Förster distance increase and luminescence signal decrease. *B*) The BRET signal was decreased after cells were treated with 1 μM TM5 peptide acting as control. *C*) Dose response curves for 5 verified BRET assay hits, with corresponding EC₅₀ concentrations ranging from 320 μM to 2.4 nM. Error bars, sd of triplicate readings. BRET (530/480 nm) luminescence units were normalized as % of Rh dimers (DMSO-treated HEK293 opsin Rluc/Venus readouts were set as 100% Rh dimer composition).

Stereospecific UV-absorbance changes of Rh

To evaluate the binding properties of the identified hit compounds with Rh, we performed photobleaching studies using UV-visible spectroscopy to measure the formation and decay of Rh photointermediates (54). The interactions of different detergents (LMNG, DDM, and CHAPS) with Rh resulted in changes in the kinetics of Meta II formation (Supplemental Fig. S7) (55). DDM solubilized Rh exhibited a complete transition from ground state to the Meta II state after illumination. As a result of this observation, 1 mM DDM was used as the optimal

detergent, retaining the dimeric organization and function of Rh (27). The enantiomers of econazole and sulconazole were separated using an OD chiral stationary-phase column to evaluate their stereospecific effects on Rh photoactivation (Fig. 4A, B) (40, 56). Stereospecific binding of the separated enantiomers to Rh was evaluated initially by measuring the Meta II formation upon photobleaching. Rh concentration used for all photobleaching experiments was 1.36 μM and a ratio of 1:36.7 was established for econazole and sulconazole enantiomer treatment. The concentration of Rh and the detergent composition greatly affects dimerization. Gel filtration elution profiles of

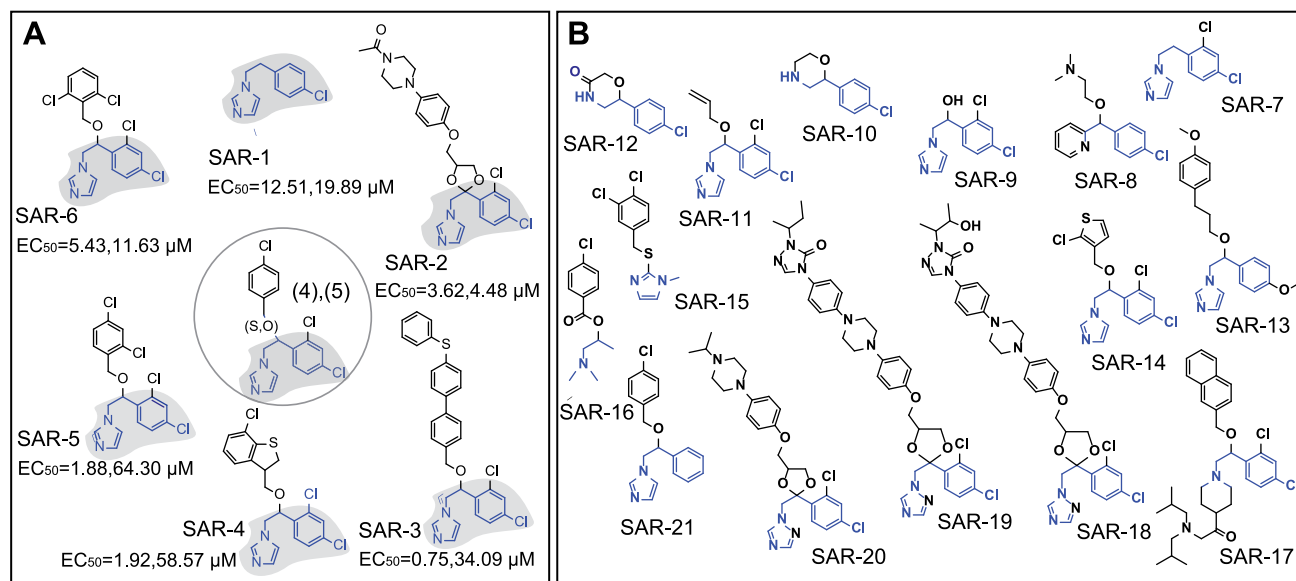


Figure 3. Chemical structures of econazole and sulconazole derivatives. *A*) Chemical structures from SAR studies identified active compounds combining β -gal complementation, and BRET and galactosidase assays. Six newly derived compounds were identified sharing a 1-(4-chlorophenethyl)-1H-imidazole (highlighted in gray) scaffold with corresponding β -gal and BRET EC_{50} values, respectively. *B*) Chemical structures of 15 inactive derivatives of econazole and sulconazole with partial 1-(4-chlorophenethyl)-1H-imidazole scaffold properties (blue).

bovine Rh revealed that buffer containing 1 mM DDM maintained the Rh dimeric state. An increased concentration of 3 mM DDM shifts Rh from the dimeric to the monomeric state (26). Therefore, we maintained 1 mM detergent composition to mimic the dimeric state of Rh. UV-absorption photobleaching revealed that the *R*-econazole enantiomer hindered Meta II formation and increased the stability of the Meta III state. In contrast, DMSO-treated Rh showed a complete transition of ground-state Rh to Meta II upon illumination. Treatment with either *R*-sulconazole (R5), *S*-sulconazole (S5), or *S*-econazole (S4) enantiomers had no effect on the stability of the Meta III and Meta II states (Fig. 4C–E).

The stability of the Meta III state was then evaluated after treatment with *R*-econazole by longer light irradiation (Fig. 4F). The absorption spectrum of Rh no longer changed with time, confirming that the peak at 465 nm does not originate from a small population of dark-state Rh but rather the Meta III stabilized state. To eliminate the possibility that the *R*-econazole enantiomer blocks all-*trans*-retinal release from the chromophore-binding pocket, hydroxylamine was added to monitor the Schiff base hydrolysis in the presence and absence of *R*-econazole (Supplemental Fig. S8) (57). The release of all-*trans*-retinal in both DMSO-treated and *R*-econazole-treated Rh suggested that *R*-econazole did not inhibit the release of all-*trans*-retinal from the chromophore-binding pocket.

Similarly, all racemic derivatives of compound econazole were tested for their interaction with Rh using UV-absorption spectroscopy. None of these compounds affected the spectral properties of Rh upon illumination (Supplemental Fig. S9). Interestingly, chemical structure comparisons revealed highly specific Rh UV-absorbance changes with *R*-econazole-treated Rh. Mild structural changes, such as substitution of an etheric bond to a

sulfuric bond, abolished the stabilized 465 nm pigment identified as Meta III probably due to the higher polar binding preference of the oxygen atom compared with the sulfur atom (58).

Functional characteristics of Rh

Next, the Meta II decay rates were compared in the presence of either *R*-econazole or *S*-econazole enantiomers followed by photoactivation. Tryptophan (Trp) fluorescence was measured to assess the rate of all-*trans*-retinal release by measuring the light-induced increase in Trp265 intrinsic fluorescence that occurs upon the release of chromophore (59). The fluorescence increase occurs due to the conformational changes associated with the release of all-*trans*-retinal, and quenching of the fluorescence either arises *via* the energy transfer to the chromophore (60) or *via* π - π interactions with Trp265. The *R*-econazole enantiomer was found to completely quench the increase in the fluorescent signal as compared with either DMSO- or *S*-econazole-treated Rh. (Fig. 5). This result suggested that Trp265 continued to interact *via* a π - π substituted interaction with the *R*-econazole enantiomer carrying 3 aromatic rings (2 phenyl rings and 1 imidazole ring) or the fluorescence of Trp265 is quenched by energy transfer to the chromophore likely due to retention of retinal in the chromophore-binding pocket. Moreover, allosteric binding also could be possible for *S*-econazole, which demonstrated decreased rates of Meta II decay compared with DMSO-treated Rh.

Next, the G_t activation efficiency of Rh was measured in the presence of either *R*-econazole or *S*-econazole. The assay monitored the intrinsic Trp fluorescence increase of the α subunit of G_t in the presence of light-activated Rh. No

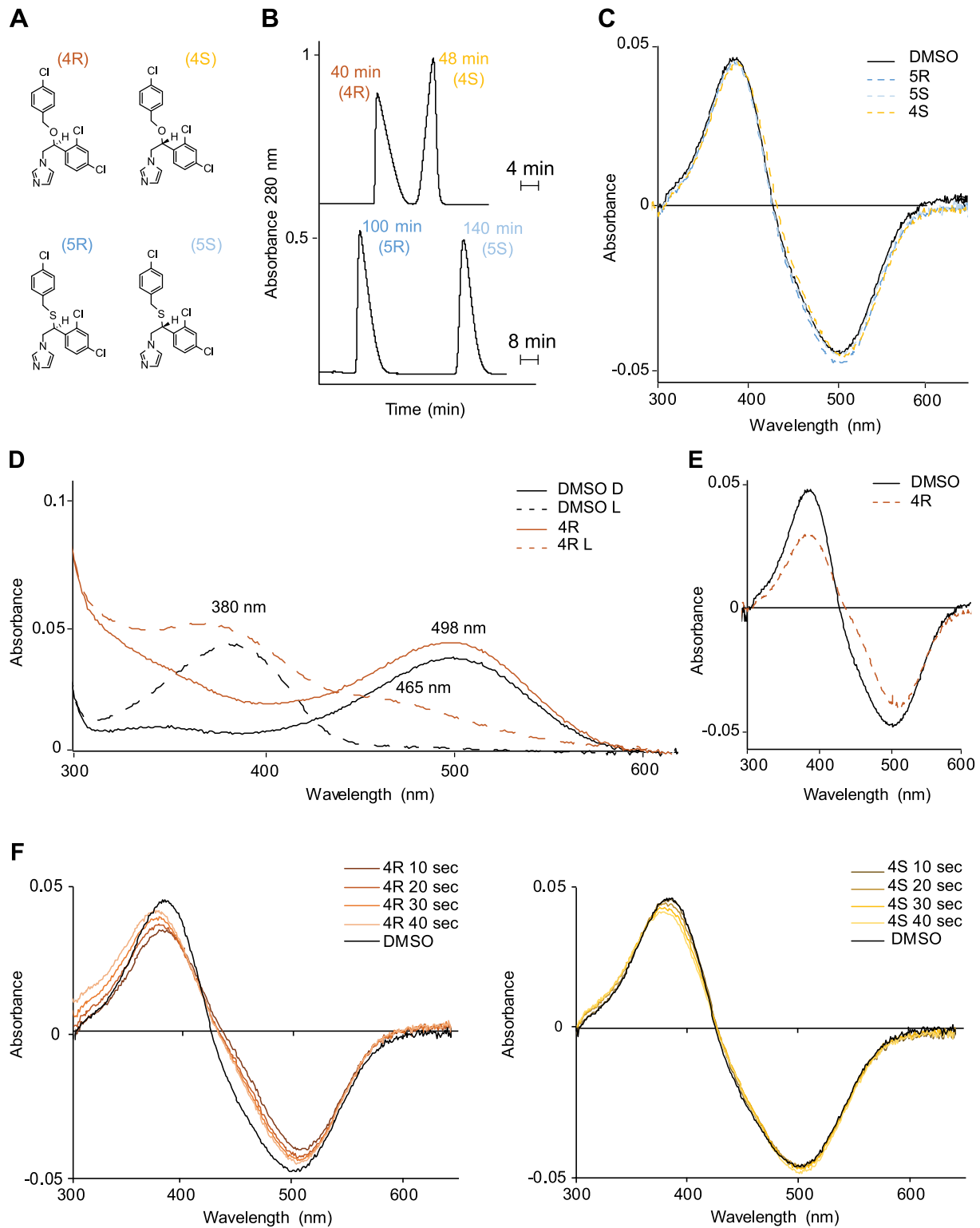


Figure 4. Stereospecific binding effect on UV-absorption spectra of dark and irradiated bovine Rh. *A*) Chemical structures of econazole and sulconazole enantiomers. *B*) Chromatograms showing the resolution of enantiomers of econazole and sulconazole on a Chiralcel OD column using hexane-2-propanol-diethylamine (485:14:1, v/v/v) as the mobile phase with a 1 ml/min flow rate. *C*) Calculated differences in spectra obtained by subtracting the light spectrum from the dark spectrum of Rh treated with *R*-sulconazole (blue), *S*-sulconazole (cyan) and *Se*conazole (yellow) in 1 mM DDM. *D*) UV-visible absorption spectra of *R*-econazole- and DMSO-treated Rh before (orange, black solid line) and after 10 s light exposure (orange, black dashed line); the pigment treated with *R*-econazole is converted to a mixture of Meta II (λ_{\max} : 380 nm) and Meta III (λ_{\max} : 465 nm) demonstrating the stereospecific binding of *R*-econazole effects on the transition of Rh from dark state to the intermediate states. *E*) Difference spectra of Rh treated with *R*-econazole (orange) and DMSO (black). *F*) Time-resolved difference absorption spectra of Rh treated with either *R*-econazole (orange), *Se*conazole (yellow), or DMSO (black), before and after exposure to bright light ranging from 10 to 40 s. 4R, *R*-econazole; 4S, with *Se*conazole; 5R, *R*-sulconazole; 5S, *S*-sulconazole.

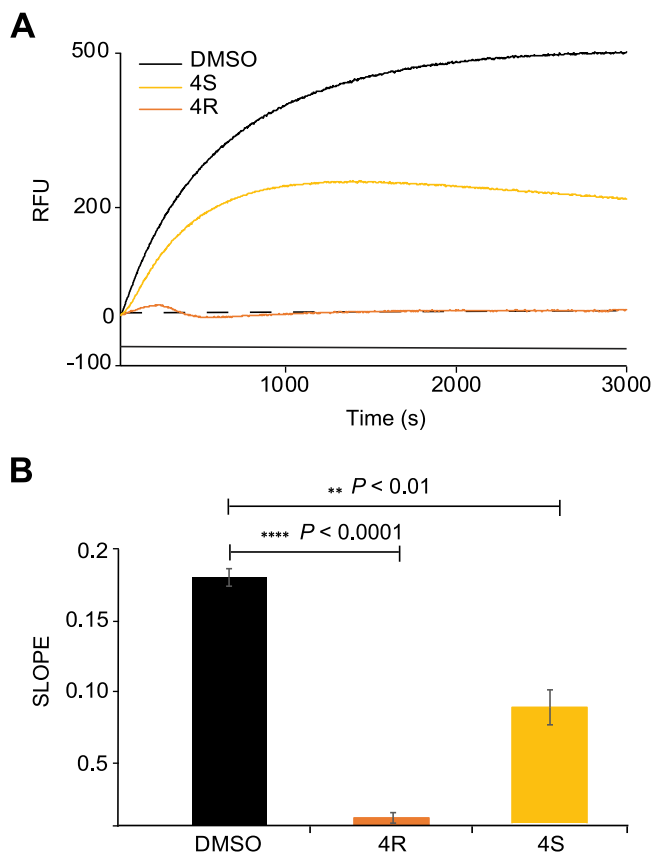


Figure 5. Rh fluorescence enhancement response. *A*) Meta II decay kinetics of Rh treated with either *R*-econazole, *S*-econazole, or DMSO in relative fluorescence units (RFU). *B*) A bar graph displaying the Meta II decay rates of Rh Meta II/III decay calculated by the slopes of curves in *A* over a prolonged time after light exposure (2000 s). DMSO, black; *S*-econazole, yellow; and *R*-econazole, orange. Columns and error bars are means \pm SD from 3 biologic repeats. Compounds *R*-econazole and *S*-econazole compared with DMSO-treated Rh demonstrated statistically significant signal reduction ($P < 0.0001$, $P < 0.01$, respectively). Statistical significance was calculated with Student's *t* test. 4R, *R*-econazole; 4S, with *S*-econazole.

significant changes were observed in G-protein activation efficiencies of Rh treated with either *R*-econazole or *S*-econazole as compared with DMSO-treated Rh (Fig. 6). This result suggested that the binding of *R*-econazole did not affect Rh-G_t complex formation, and that the *R*-econazole-bound Rh remained functional. These findings are consistent with previous studies that both monomeric and dimeric Rh activate G_t (30).

Although *R*-econazole or *S*-econazole did not affect the activation of G_t by Rh in the *in vitro* assay, it is nonetheless possible that Rh dimerization still plays a role during phototransduction in intact photoreceptor cells. This possibility was tested by determining the effect of *R*-econazole and *S*-econazole on rod photoreceptor light responses by using *ex vivo* electroretinography of isolated wild-type mouse retinas (Fig. 7A). Experiments were performed in which light responses of rods were compared between retinas incubated for 5–6 h in control solution or in Ames' containing a 500 μ M mixture of *R*- and *S*-forms of econazole. Incubation in econazole decreased the r_{\max} of light

responses and decreased the sensitivity of rods to light (Fig. 7B). To determine the stereospecificity of econazole, the same experiment was performed, incubating the retinas either in 500 μ M *R*-econazole or *S*-econazole. Interestingly, *R*-econazole did not decrease the r_{\max} of rods but slowed their response kinetics (Fig. 7C), whereas *S*-econazole decreased r_{\max} and the sensitivity of rods significantly but did not affect light response kinetics (Fig. 7D). These findings indicate that econazole enantiomers are stereospecific modulators effecting the photoreceptor light responses by slowing or decreasing the signal.

DISCUSSION

In this study, we demonstrate a robust and high-throughput cell-based β -gal complementation assay capable of identifying compounds that modulate Rh dimerization. The issue of receptor orientation for any GPCR in a cell-based dimerization assay when compared with the native environment has been addressed quantitatively only once, for β -2 adrenergic receptor (β 2AR) (61). In that study, the possibility that random interactions were responsible for dimerization was refuted. When Rh is transported to the cell membrane, its topology is determined by its peptide sequence. Furthermore, Rh dimerization is not affected by fusion proteins due to the length of the linker between Rh and EA/PK. Thus, the orientation of Rh dimers would be similar in our assay and in ROS and driven by thermodynamics. This β -gal complementary assay identified 9 hits acting as Rh dimerization disrupters *in vitro*. Using an independent BRET-based complementary assay, a β -gal activity counter screen, and a cell viability assay, we reduced false-positives among the initial hits leading to 2 final compounds econazole and sulconazole. Our preliminary SAR study yielded 6 derivative compounds of econazole and sulconazole that disrupted Rh dimerization in a dose-dependent manner according to both of the dimerization cell-based assays. Notably, the most promising derivative (SAR 2), a racemate with 2 chiral centers on the acetal ring sharing the 1-(4-chlorophenethyl)-1H-imidazole scaffold with lipophilic properties, demonstrated the highest *in vitro* potency among all compounds screened. All hits were subjected to Rh photobleaching analysis in which only econazole showed perturbations either at an allosteric site or at the chromophore-binding site of Rh. Although racemic compounds have similar chemical structures, most enantiomers exhibit differences in biologic activities (62). Therefore, to obtain insight into the stereospecific binding to Rh and by extension rod light responses after photoisomerization, econazole enantiomers were separated and assessed *in vitro* and *ex vivo*.

The separated *R*-enantiomer affected the transition from Meta II to Meta III photointermediates of Rh as observed by UV-visible absorption spectroscopy. We found that *R*-econazole binding stabilizes the Meta III state, whereas *S*-econazole has no effect on the formation of photointermediates. These findings indicate that *R*-econazole is a stereospecific binder that effects Meta II and Meta III formation. Stabilization of Meta III *via* direct binding of this compound to Rh can then indirectly

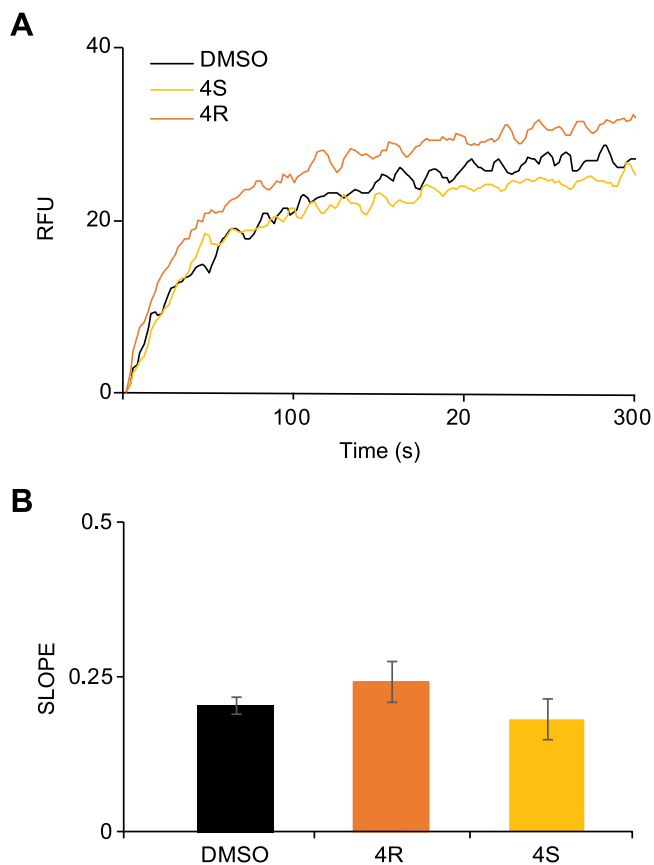


Figure 6. Transductin (G_t) activation assay. *A*) Comparison of G_t activation efficiencies of DMSO- (black), *R*-econazole- (orange), or *S*-econazole- (yellow) treated Rh. *B*) A bar graph showing the initial rates of G_t activation for Rh treated with either *R*-econazole, *S*-econazole, or DMSO. Columns and error bars are means \pm SD from 3 biologic repeats. A statistically significant difference was not observed between the tested samples. Statistical significance was calculated with Student's *t* test. 4R, *R*-econazole; 4S, with *S*-econazole

interfere with dimerization by imposing protein conformational changes that affect the ability of Rh to dimerize. Previous studies reported that TM helices 1 and 7–8 form the dimer interface for Rh (30, 63–65). Therefore, conformational constraints to the TM contact helices *via* binding of *R*-econazole could interfere with the proper protein conformational changes that occur during photobleaching and indirectly affect dimerization. It is important to mention that all photobleaching experiments were performed by using Rh dissolved in 1 mM DDM imitating the oligomeric state of Rh. Performing size exclusion chromatography of Rh treated with *R*-econazole or *S*-econazole solubilized in 1 mM DDM in either higher concentrations or longer incubation time conditions, Rh precipitated suggesting a competition between the compounds and DDM. Therefore, the stabilization of Meta III and Trp265 modulation *via* binding of these compounds can indirectly interfere with dimerization. The light-induced helical rearrangement of dimeric or monomeric Rh was also previously studied by Rh reconstitution in nanodiscs (66). Findings demonstrated that dimerization affects the extent of conformational change during photobleaching and the interaction between Rh molecules modulates structural

changes. Therefore, it is likely that the disruption of Rh dimerization suppresses helical rearrangement upon photoactivation. Additionally, the stabilized Meta III population was not photoconverted to either Meta II or opsin and free retinal. This equilibrium shift between Meta I and Meta II following treatment with *R*-econazole in DDM was also observed in DMSO-treated Rh in CHAPS detergent. The possibility that the Meta III population is affected by the lipid composition was rejected because the *S*-enantiomer of compound 4 had no effect on Rh UV-absorption under the same conditions. Therefore, the stereospecificity of the *R*-enantiomer is the key element in stabilizing the 465 nm pigment. To examine the possibility that *R*-econazole imposes a closed conformation of the retinal-binding site (dark-state Rh) that blocks access of hydroxylamine to the Schiff base, we treated the *R*-econazole–Rh mixture with hydroxylamine and monitored the hydrolysis of all-*trans*-retinal. The release of all-*trans*-retinal from Rh both in the presence and absence of *R*-econazole suggested that the retinal-binding site is in its open conformation after photoactivation in the presence of *R*-econazole. Interestingly, the Trp fluorescence assay of photoactivated Rh showed that *R*-econazole completely quenches the increase in Trp265 fluorescence. Thus, implying that *R*-econazole either enters the chromophore-binding pocket and interacts with Trp265 *via* π - π stacking interactions or an allosteric binding of *R*-econazole affects the retention of retinal in the chromophore-binding pocket and causes Trp265 fluorescence quenching without effecting G-protein activation rates. Considering the Meta III stabilizing effect *in vitro*, *R*-econazole slowed the photoresponse kinetics *ex vivo*. In contrast, *S*-econazole demonstrated a strong effect on the sensitivity of rods and r_{max} without effecting photoresponse kinetics. The difference between *R*-econazole and *S*-econazole on Rh dimerization disruption was evaluated to address their effect on the electrophysiological response. In the β -gal complementation cell-based assay both compounds disrupted Rh dimerization in a dose-dependent manner; however, compound *R*-econazole caused a 2-fold lower dimer formation compared with *S*-econazole (Supplemental Fig. S10). This finding suggests that the *R*-enantiomer more effectively disrupts dimerization, supporting our conclusion that the 2 enantiomers likely have different mechanisms of action.

The notion that GPCRs function as monomers has been challenged by emerging evidence of GPCR dimerization and oligomerization necessary for proper function (23). Although research is progressing rapidly, GPCRs remain relatively untapped as targets for further pharmacological intervention. We believe the most promising aspect in this area of research lies in the potential for allosteric regulation of GPCRs (67). The allosteric regulation of GPCRs with high specificity will provide important opportunities to treat a wide range of chronic diseases. Although the underlying mechanism by which econazole disrupts Rh dimerization and its effect on Rh photointermediates requires further investigation, this study provides direct evidence for the interplay between the chromophore-binding pocket and the Rh dimer interface (30, 68–70). Future studies will focus on delineating the mechanism of Rh dimer disruption

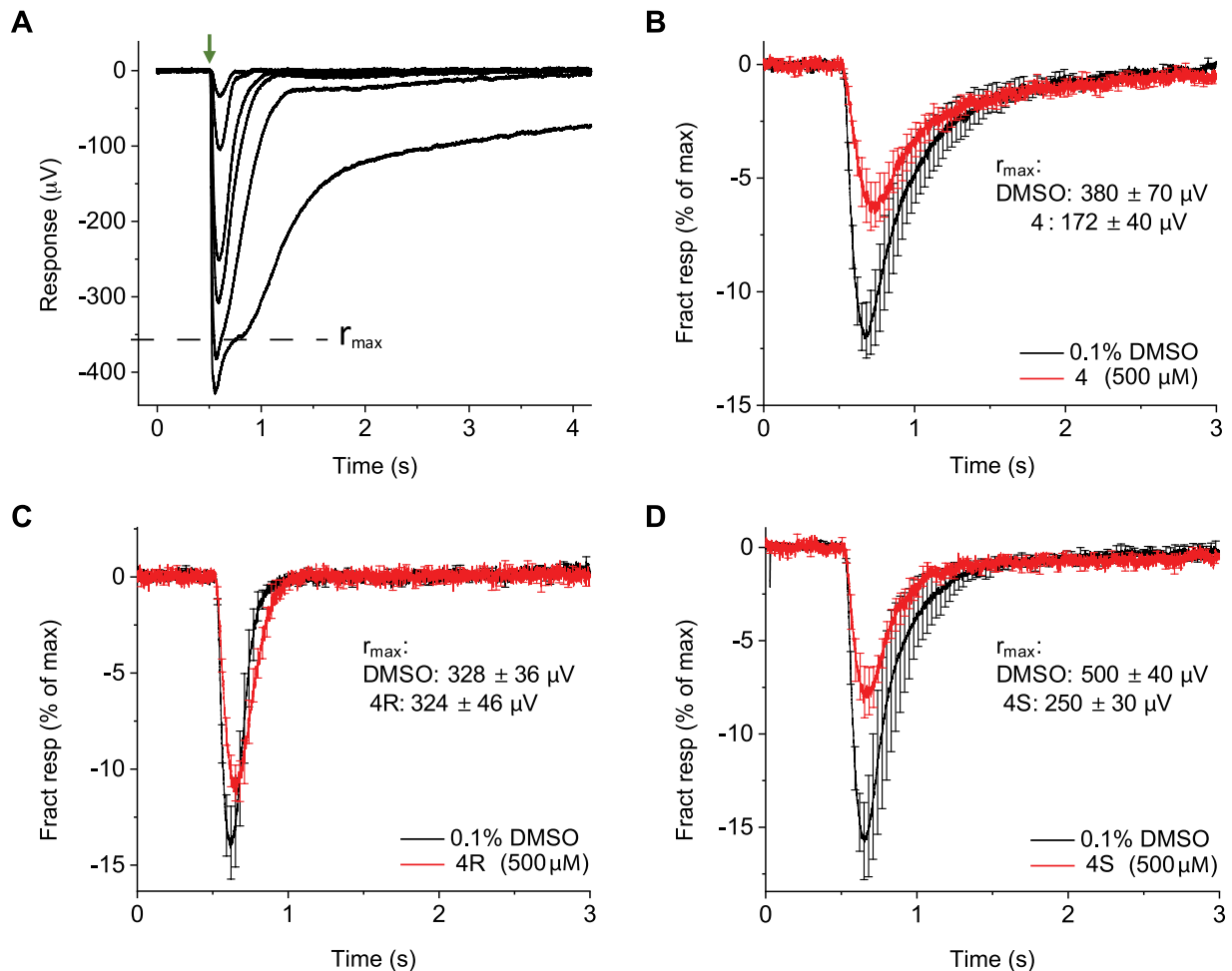


Figure 7. Effect of econazole on rod photoreceptor light response. *A*) Representative family of responses to flashes (1 ms, delivered at $t = 500$ ms) of light ranging from 100 to 4000 photons (530 nm)/ μm^2 recorded using *ex vivo* ERG from wild-type (WT) mouse retina perfused with Ames' buffer and pharmacological blockers to isolate the photoreceptor response of the ERG signal at 36°C . This retina was incubated for 5 h at room temperature in Ames' containing 0.1% DMSO before recordings. *B–D*) Mean \pm SEM response to the dimmest flash (100 photons/ μm^2) recorded from retinas after 5–6 h of incubation in control (black, 0.1% DMSO) and in 500 μM econazole (*B*), *R*-econazole (*C*), and *S*-econazole (*D*) (red). r_{max} amplitudes (mean \pm SEM) are indicated in each figure. Peak amplitudes of light responses and r_{max} from DMSO- and econazole-treated retinas were statistically different in *B* and *D*, and time-to-peaks were statistically different in *C*. 4, econazole; 4R, *R*-econazole; 4S, with *S*-econazole.

and Meta III stabilization by *R*-econazole. Overall, the HTS methodology reported here can easily be adapted to identify compounds that modulate GPCR dimerization *in vitro* and *in vivo*. Such studies will greatly benefit our current understanding of GPCR pharmacology and the critical role GPCR dimerization plays in cellular signaling. FJ

ACKNOWLEDGMENTS

The authors thank Drs. Philip Kiser (Physiology & Biophysics Department, University of California–Irvine, CA, USA), Timothy Kern (Ophthalmology Department, University of California–Irvine), and Angele Nalbandian (Ophthalmology Department, University of California–Irvine) for helpful comments on this manuscript. The authors wish to thank members of the Small Molecule Drug Development Core facilities at Case Western Reserve University for guidance through the development of our high-throughput screening (HTS) assay. This research was supported in part by grants from the U.S. National Institutes of Health (NIH) (EY R24024864 and R24EY027283 to K.P., EY024992 to Y.C., and EY026651 to F.V.), an unrestricted Research to Prevent Blindness

(RPB) grant to the Department of Ophthalmology at University of California–Irvine (UCI); the Canadian Institute for Advanced Research (CIFAR); and the Alcon Research Institute (ARI). K.P. is the Leopold Chair of Ophthalmology. The authors declare no conflicts of interest.

AUTHOR CONTRIBUTIONS

T. Getter, S. Gulati, Y. Chen, F. Vinberg, and K. Palczewski participated in the design of the research; T. Getter, S. Gulati, R. Zimmerman, and F. Vinberg conducted the experiments; T. Getter, S. Gulati, Y. Chen, and F. Vinberg contributed new reagents or analytical tools; T. Getter, S. Gulati, and F. Vinberg performed the data analysis; and T. Getter, S. Gulati, R. Zimmerman, Y. Chen, F. Vinberg, and K. Palczewski contributed to the writing of the manuscript.

REFERENCES

- Lefkowitz, R. J. (2007) Seven transmembrane receptors: something old, something new. *Acta Physiol. (Oxf.)* **190**, 9–19

2. Rosenbaum, D. M., Rasmussen, S. G., and Kobilka, B. K. (2009) The structure and function of G-protein-coupled receptors. *Nature* **459**, 356–363
3. Salon, J. A., Lodowski, D. T., and Palczewski, K. (2011) The significance of G protein-coupled receptor crystallography for drug discovery. *Pharmacol. Rev.* **63**, 901–937
4. Mustafi, D., and Palczewski, K. (2009) Topology of class A G protein-coupled receptors: insights gained from crystal structures of rhodopsins, adrenergic and adenosine receptors. *Mol. Pharmacol.* **75**, 1–12
5. Overington, J. P., Al-Lazikani, B., and Hopkins, A. L. (2006) How many drug targets are there? *Nat. Rev. Drug Discov.* **5**, 993–996
6. Lefkowitz, R. J., and Shenoy, S. K. (2005) Transduction of receptor signals by beta-arrestins. *Science* **308**, 512–517
7. Luttrell, L. M., and Lefkowitz, R. J. (2002) The role of beta-arrestins in the termination and transduction of G-protein-coupled receptor signals. *J. Cell Sci.* **115**, 455–465
8. Azzi, M., Charest, P. G., Angers, S., Rousseau, G., Kohout, T., Bouvier, M., and Pineyro, G. (2003) Beta-arrestin-mediated activation of MAPK by inverse agonists reveals distinct active conformations for G protein-coupled receptors. *Proc. Natl. Acad. Sci. USA* **100**, 11406–11411
9. Palczewski, K. (2006) G protein-coupled receptor rhodopsin. *Annu. Rev. Biochem.* **75**, 743–767
10. Shichida, Y., and Imai, H. (1998) Visual pigment: G-protein-coupled receptor for light signals. *Cell. Mol. Life Sci.* **54**, 1299–1315
11. Kandori, H., Shichida, Y., and Yoshizawa, T. (2001) Photoisomerization in rhodopsin. *Biochemistry (Mosc.)* **66**, 1197–1209
12. Fung, B. K., Hurley, J. B., and Stryer, L. (1981) Flow of information in the light-triggered cyclic nucleotide cascade of vision. *Proc. Natl. Acad. Sci. USA* **78**, 152–156
13. König, B., Welte, W., and Hofmann, K. P. (1989) Photoactivation of rhodopsin and interaction with transducin in detergent micelles. Effect of 'doping' with steroid molecules. *FEBS Lett.* **257**, 163–166
14. Ramon, E., Marron, J., del Valle, L., Bosch, L., Andrés, A., Manyosa, J., and Garriga, P. (2003) Effect of dodecyl maltoside detergent on rhodopsin stability and function. *Vision Res.* **43**, 3055–3061
15. Bartl, F. J., and Vogel, R. (2007) Structural and functional properties of metarhodopsin III: recent spectroscopic studies on deactivation pathways of rhodopsin. *Phys. Chem. Chem. Phys.* **9**, 1648–1658
16. Pin, J. P., Neubig, R., Bouvier, M., Devi, L., Filizola, M., Javitch, J. A., Lohse, M. J., Milligan, G., Palczewski, K., Parmentier, M., and Spedding, M. (2007) International Union of Basic and Clinical Pharmacology. LXVII. Recommendations for the recognition and nomenclature of G protein-coupled receptor heteromultimers. *Pharmacol. Rev.* **59**, 5–13
17. Palczewski, K. (2010) Oligomeric forms of G protein-coupled receptors (GPCRs). *Trends Biochem. Sci.* **35**, 595–600
18. Fotiadis, D., Liang, Y., Filipek, S., Saperstein, D. A., Engel, A., and Palczewski, K. (2003) Atomic-force microscopy: rhodopsin dimers in native disc membranes. *Nature* **421**, 127–128
19. Fotiadis, D., Liang, Y., Filipek, S., Saperstein, D. A., Engel, A., and Palczewski, K. (2004) The G protein-coupled receptor rhodopsin in the native membrane. *FEBS Lett.* **564**, 281–288
20. Liang, Y., Fotiadis, D., Filipek, S., Saperstein, D. A., Palczewski, K., and Engel, A. (2003) Organization of the G protein-coupled receptors rhodopsin and opsin in native membranes. *J. Biol. Chem.* **278**, 21655–21662
21. Liang, Y., Fotiadis, D., Maeda, T., Maeda, A., Modzelewska, A., Filipek, S., Saperstein, D. A., Engel, A., and Palczewski, K. (2004) Rhodopsin signaling and organization in heterozygote rhodopsin knockout mice. *J. Biol. Chem.* **279**, 48189–48196
22. Gunkel, M., Schöneberg, J., Alkhalidi, W., Irsen, S., Noé, F., Kaupp, U. B., and Al-Amoudi, A. (2015) Higher-order architecture of rhodopsin in intact photoreceptors and its implication for photo-transduction kinetics. *Structure* **23**, 628–638
23. Whorton, M. R., Jastrzebska, B., Park, P. S., Fotiadis, D., Engel, A., Palczewski, K., and Sunahara, R. K. (2008) Efficient coupling of transducin to monomeric rhodopsin in a phospholipid bilayer. *J. Biol. Chem.* **283**, 4387–4394
24. Nemoto, W., and Toh, H. (2005) Prediction of interfaces for oligomerizations of G-protein coupled receptors. *Proteins* **58**, 644–660
25. Simpson, L. M., Taddese, B., Wall, I. D., and Reynolds, C. A. (2010) Bioinformatics and molecular modelling approaches to GPCR oligomerization. *Curr. Opin. Pharmacol.* **10**, 30–37
26. Jastrzebska, B., Chen, Y., Orban, T., Jin, H., Hofmann, L., and Palczewski, K. (2015) Disruption of rhodopsin dimerization with synthetic peptides targeting an interaction interface. *J. Biol. Chem.* **290**, 25728–25744
27. Jastrzebska, B., Ringler, P., Palczewski, K., and Engel, A. (2013) The rhodopsin-transducin complex houses two distinct rhodopsin molecules. *J. Struct. Biol.* **182**, 164–172
28. Jastrzebska, B., Orban, T., Golczak, M., Engel, A., and Palczewski, K. (2013) Asymmetry of the rhodopsin dimer in complex with transducin. *FASEB J.* **27**, 1572–1584
29. Jastrzebska, B., Ringler, P., Lodowski, D. T., Moiseenkova-Bell, V., Golczak, M., Müller, S. A., Palczewski, K., and Engel, A. (2011) Rhodopsin-transducin heteropentamer: three-dimensional structure and biochemical characterization. *J. Struct. Biol.* **176**, 387–394
30. Ploier, B., Caro, L. N., Morizumi, T., Pandey, K., Pearing, J. N., Goren, M. A., Finnemann, S. C., Graumann, J., Arshavsky, V. Y., Dittman, J. S., Ernst, O. P., and Menon, A. K. (2016) Dimerization deficiency of enigmatic retinitis pigmentosa-linked rhodopsin mutants. *Nat. Commun.* **7**, 12832
31. Macke, J. P., Davenport, C. M., Jacobson, S. G., Hennessey, J. C., Gonzalez-Fernandez, F., Conway, B. P., Heckenlively, J., Palmer, R., Maumenee, I. H., Sieving, P., Gouras, P., Good, W., and Nathans, J. (1993) Identification of novel rhodopsin mutations responsible for retinitis pigmentosa: implications for the structure and function of rhodopsin. *Am. J. Hum. Genet.* **53**, 80–89
32. Chen, Y., Tang, H., Seibel, W., Papoian, R., Li, X., Lambert, N. A., and Palczewski, K. (2015) A high-throughput drug screening strategy for detecting rhodopsin P23H mutant rescue and degradation. *Invest. Ophthalmol. Vis. Sci.* **56**, 2553–2567
33. Zhang, J. H., Chung, T. D., and Oldenburg, K. R. (1999) A simple statistical parameter for use in evaluation and validation of high throughput screening assays. *J. Biomol. Screen.* **4**, 67–73
34. Levi, J., De, A., Cheng, Z., and Gambhir, S. S. (2007) Bisdeoxycoelenterazine derivatives for improvement of bioluminescence resonance energy transfer assays. *J. Am. Chem. Soc.* **129**, 11900–11901
35. Miranda, O. R., Chen, H. T., You, C. C., Mortenson, D. E., Yang, X. C., Bunz, U. H., and Rotello, V. M. (2010) Enzyme-amplified array sensing of proteins in solution and in biofluids. *J. Am. Chem. Soc.* **132**, 5285–5289
36. Papermaster, D. S. (1982) Preparation of retinal rod outer segments. *Methods Enzymol.* **81**, 48–52
37. Baker, B. Y., Gulati, S., Shi, W., Wang, B., Stewart, P. L., and Palczewski, K. (2015) Crystallization of proteins from crude bovine rod outer segments. *Methods Enzymol.* **557**, 439–458
38. Gulati, S., Jastrzebska, B., Banerjee, S., Placeres, A. L., Miszta, P., Gao, S., Gunderson, K., Tochtrop, G. P., Filipek, S., Katayama, K., Kiser, P. D., Mogi, M., Stewart, P. L., and Palczewski, K. (2017) Photocyclic behavior of rhodopsin induced by an atypical isomerization mechanism. *Proc. Natl. Acad. Sci. USA* **114**, E2608–E2615
39. Hofmann, L., Gulati, S., Sears, A., Stewart, P. L., and Palczewski, K. (2016) An effective thiol-reactive probe for differential scanning fluorimetry with a standard real-time polymerase chain reaction device. *Anal. Biochem.* **499**, 63–65
40. Aboul-Enein, H. Y., and Ali, I. (2002) Comparative study of the enantiomeric resolution of chiral antifungal drugs econazole, miconazole and sulconazole by HPLC on various cellulose chiral columns in normal phase mode. *J. Pharm. Biomed. Anal.* **27**, 441–446
41. Sakmar, T. P., Franke, R. R., and Khorana, H. G. (1991) The role of the retinylidene Schiff base counterion in rhodopsin in determining wavelength absorbance and Schiff base pKa. *Proc. Natl. Acad. Sci. USA* **88**, 3079–3083
42. Gulati, S., Jin, H., Masuho, I., Orban, T., Cai, Y., Pardon, E., Martemyanov, K. A., Kiser, P. D., Stewart, P. L., Ford, C. P., Steyaert, J., and Palczewski, K. (2018) Targeting G protein-coupled receptor signaling at the G protein level with a selective nanobody inhibitor. *Nat. Commun.* **9**, 1996
43. Fahmy, K., and Sakmar, T. P. (1993) Regulation of the rhodopsin-transducin interaction by a highly conserved carboxylic acid group. *Biochemistry* **32**, 7229–7236
44. Heck, M., and Hofmann, K. P. (2001) Maximal rate and nucleotide dependence of rhodopsin-catalyzed transducin activation: initial rate analysis based on a double displacement mechanism. *J. Biol. Chem.* **276**, 10000–10009
45. Vinberg, F., Wang, T., Molday, R. S., Chen, J., and Kefalov, V. J. (2015) A new mouse model for stationary night blindness with mutant *Slc24a1* explains the pathophysiology of the associated human disease. *Hum. Mol. Genet.* **24**, 5915–5929

46. Vinberg, F., Kolesnikov, A. V., and Kefalov, V. J. (2014) Ex vivo ERG analysis of photoreceptors using an in vivo ERG system. *Vision Res.* **101**, 108–117
47. Chen, Y., and Tang, H. (2015) High-throughput screening assays to identify small molecules preventing photoreceptor degeneration caused by the rhodopsin P23H mutation. *Methods Mol. Biol.* **1271**, 369–390
48. Chen, Y., Chen, Y., Jastrzebska, B., Golczak, M., Gulati, S., Tang, H., Seibel, W., Li, X., Jin, H., Han, Y., Gao, S., Zhang, J., Liu, X., Heidari-Torkabadi, H., Stewart, P. L., Harte, W. E., Tochtrop, G. P., and Palczewski, K. (2018) A novel small molecule chaperone of rod opsin and its potential therapy for retinal degeneration. *Nat. Commun.* **9**, 1976
49. James, J. R., Oliveira, M. I., Carmo, A. M., Iaboni, A., and Davis, S. J. (2006) A rigorous experimental framework for detecting protein oligomerization using bioluminescence resonance energy transfer. *Nat. Methods* **3**, 1001–1006
50. Pflieger, K. D., Seeber, R. M., and Eidne, K. A. (2006) Bioluminescence resonance energy transfer (BRET) for the real-time detection of protein-protein interactions. *Nat. Protoc.* **1**, 337–345
51. Otto-Duessel, M., Khankaldyyan, V., Gonzalez-Gomez, I., Jensen, M. C., Laug, W. E., and Rosol, M. (2006) In vivo testing of Renilla luciferase substrate analogs in an orthotopic murine model of human glioblastoma. *Mol. Imaging* **5**, 57–64
52. Baldini, L., Wilson, A. J., Hong, J., and Hamilton, A. D. (2004) Pattern-based detection of different proteins using an array of fluorescent protein surface receptors. *J. Am. Chem. Soc.* **126**, 5656–5657
53. Crouch, S. P., Kozlowski, R., Slater, K. J., and Fletcher, J. (1993) The use of ATP bioluminescence as a measure of cell proliferation and cytotoxicity. *J. Immunol. Methods* **160**, 81–88
54. Kojima, K., Imamoto, Y., Maeda, R., Yamashita, T., and Shichida, Y. (2014) Rod visual pigment optimizes active state to achieve efficient G protein activation as compared with cone visual pigments. *J. Biol. Chem.* **289**, 5061–5073
55. Schleicher, A., Franke, R., Hofmann, K. P., Finkelmann, H., and Welte, W. (1987) Deoxylysolecithin and a new biphenyl detergent as solubilizing agents for bovine rhodopsin. Functional test by formation of metarhodopsin II and binding of G-protein. *Biochemistry* **26**, 5908–5916
56. Chankvetadze, B., Chankvetadze, L., Sidamonidze, S., Yashima, E., and Okamoto, Y. (1996) High performance liquid chromatography enantioseparation of chiral pharmaceuticals using tris(chloromethylphenylcarbamate)s of cellulose. *J. Pharm. Biomed. Anal.* **14**, 1295–1303
57. Janz, J. M., and Farrens, D. L. (2004) Role of the retinal hydrogen bond network in rhodopsin Schiff base stability and hydrolysis. *J. Biol. Chem.* **279**, 55886–55894
58. Saeva, F. D., and Olin, G. R. (1980) Electron-donating properties of oxygen vs. sulfur. Redox potentials for some pyrylium and thiapyrylium salts. *J. Am. Chem. Soc.* **102**, 299–303
59. Farrens, D. L., and Khorana, H. G. (1995) Structure and function in rhodopsin. Measurement of the rate of metarhodopsin II decay by fluorescence spectroscopy. *J. Biol. Chem.* **270**, 5073–5076
60. Alexiev, U., and Farrens, D. L. (2014) Fluorescence spectroscopy of rhodopsins: insights and approaches. *Biochim. Biophys. Acta* **1837**, 694–709
61. Mercier, J. F., Salahpour, A., Angers, S., Breit, A., and Bouvier, M. (2002) Quantitative assessment of beta 1- and beta 2-adrenergic receptor homo- and heterodimerization by bioluminescence resonance energy transfer. *J. Biol. Chem.* **277**, 44925–44931
62. Nguyen, L. A., He, H., and Pham-Huy, C. (2006) Chiral drugs: an overview. *Int. J. Biomed. Sci.* **2**, 85–100
63. Knepp, A. M., Periole, X., Marrink, S. J., Sakmar, T. P., and Huber, T. (2012) Rhodopsin forms a dimer with cytoplasmic helix 8 contacts in native membranes. *Biochemistry* **51**, 1819–1821
64. Salom, D., Lodowski, D. T., Stenkamp, R. E., Le Trong, I., Golczak, M., Jastrzebska, B., Harris, T., Ballesteros, J. A., and Palczewski, K. (2006) Crystal structure of a photoactivated deprotonated intermediate of rhodopsin. *Proc. Natl. Acad. Sci. USA* **103**, 16123–16128
65. Zhang, T., Cao, L. H., Kumar, S., Enemchukwu, N. O., Zhang, N., Lambert, A., Zhao, X., Jones, A., Wang, S., Dennis, E. M., Fnu, A., Ham, S., Rainier, J., Yau, K. W., and Fu, Y. (2016) Dimerization of visual pigments in vivo. *Proc. Natl. Acad. Sci. USA* **113**, 9093–9098
66. Imamoto, Y., Kojima, K., Oka, T., Maeda, R., and Shichida, Y. (2015) Helical rearrangement of photoactivated rhodopsin in monomeric and dimeric forms probed by high-angle X-ray scattering. *Photochem. Photobiol. Sci.* **14**, 1965–1973
67. Lane, J. R., Abdul-Ridha, A., and Canals, M. (2013) Regulation of G protein-coupled receptors by allosteric ligands. *ACS Chem. Neurosci.* **4**, 527–534
68. Jastrzebska, B., Maeda, T., Zhu, L., Fotiadis, D., Filipek, S., Engel, A., Stenkamp, R. E., and Palczewski, K. (2004) Functional characterization of rhodopsin monomers and dimers in detergents. *J. Biol. Chem.* **279**, 54663–54675
69. Periole, X., Knepp, A. M., Sakmar, T. P., Marrink, S. J., and Huber, T. (2012) Structural determinants of the supramolecular organization of G protein-coupled receptors in bilayers. *J. Am. Chem. Soc.* **134**, 10959–10965
70. Fotiadis, D., Jastrzebska, B., Philippsen, A., Müller, D. J., Palczewski, K., and Engel, A. (2006) Structure of the rhodopsin dimer: a working model for G-protein-coupled receptors. *Curr. Opin. Struct. Biol.* **16**, 252–259

Received for publication February 14, 2019.

Accepted for publication April 23, 2019.